



CrossMark
click for updates

Cite this: *RSC Adv.*, 2015, 5, 52066

Catalytic oxidation of toluene over a porous Co_3O_4 -supported ruthenium catalyst†

Xiaolong Liu,^a Jian Wang,^{ab} Junlin Zeng,^{ac} Xue Wang^a and Tingyu Zhu^{*a}

Porous Co_3O_4 -MOF and $\text{Ru}/\text{Co}_3\text{O}_4$ -MOF were prepared through a metal-organic frameworks (MOFs)-templated method, and the bulk materials resulted from precipitation method were prepared for comparison. All catalysts were tested for the catalytic oxidation of toluene in the temperature range of 150–300 °C, and $\text{Ru}/\text{Co}_3\text{O}_4$ -MOF showed apparently higher catalytic activity and CO_2 selectivity than other materials. The influence of water vapour on the catalytic oxidation of toluene was studied at 235 °C and 245 °C, and it could be found that the inhibition effect weakened with the increase of temperature. Additionally, the test of 12 h on-stream reaction was conducted to explore the stability of $\text{Ru}/\text{Co}_3\text{O}_4$ -MOF.

Received 19th April 2015

Accepted 8th June 2015

DOI: 10.1039/c5ra07072d

www.rsc.org/advances

1. Introduction

Volatile organic compounds (VOCs) emitted from industrial processes and transportation activities are considered as great contributors to air pollution and dangerous to human health.^{1–3} The most common approaches for VOCs removal include thermal incineration, catalytic oxidation, biochemical methods, adsorption strategies, and other techniques.^{4–9} Due to its advantages of high efficiency, low temperature, and high selectivity to harmless products, catalytic oxidation is regarded as a promising pathway to reduce VOCs emissions to meet the standards of air pollution control regulations.^{10,11} In recent years, various catalysts have been used for the complete oxidation of VOCs, such as noble metals,^{11–15} transition metal oxides,^{16–20} and perovskite-type oxides.^{21–25} Supported platinum and palladium materials are well established as efficient catalysts for complete oxidation of VOCs,^{26–30} whereas their wide applications are limited due to the high costs. Transition metal oxides have been increasingly studied as the catalysts for oxidation of VOCs in single or mixed metal oxides formations,^{31–33} usually showing lower catalytic activities than noble metals. Recently, they have been used as supports or additives for platinum, palladium, and gold-based catalysts in many cases.^{34–37}

Ruthenium catalysts have received considerable importance in CO oxidation,^{38,39} deacon process,^{40,41} and catalytic oxidation of VOCs.^{42–44} Nevertheless, ruthenium-based materials catalyzed VOCs oxidations are far less investigated compared to other noble metals. In the reports on Ru promoted oxidation of VOCs, ethyl acetate,⁴⁵ propane,^{46–48} toluene,^{42,49} and chlorobenzene^{50–53} could be totally oxidized within the temperature range of 175–275 °C. Noteworthy, Mitsui *et al.* compared the catalytic performance of CeO_2 supported noble metals in oxidation of ethyl acetate, such as Ru, Pt, Pd, and Rh, respectively, and found that Ru containing catalyst exhibited the highest catalytic activity.⁵⁴

Spinel cobalt oxide (Co_3O_4) has been well established as an intriguing material in the complete oxidation of VOCs, and its outstanding catalytic activity was mostly attributed to the mobile oxygen within the Co_3O_4 structure.^{55–58} In the field of catalytic oxidation of VOCs, it is generally concluded that the efficiency of the catalyst is greatly concerned with the oxygen vacancy, redox ability, and some morphological factors such as surface area and porous structure.^{59–62} Accordingly, various nanocasting strategies were developed to modify the structures of the catalysts, and Co_3O_4 with different nanostructures, such as nanoflowers, nanorods, and nanotubes, have been prepared.^{58,63}

In recent years, metal-organic frameworks (MOFs) have emerged as promising sacrificial templates for fabricating hierarchically porous metal oxides through solid-state thermolysis method.^{64–67} As compared to other templates, MOFs exhibit the advantages of high porosity, large surface area, long-range ordering structure, and easily removable properties under controlled calcinations conditions. Through MOFs-templated method, various metal oxides have been prepared and employed in different research fields, such as spindle-like mesoporous $\alpha\text{-Fe}_2\text{O}_3$ as lithium-ion battery anode materials⁶⁴

^aBeijing Engineering Research Center of Process Pollution Control, National Engineering Laboratory for Hydrometallurgical Cleaner Production Technology, Institute of Process Engineering, Chinese Academy of Sciences, Beijing 100190, China. E-mail: tyzhu@ipe.ac.cn; Fax: +86-10-82544821; Tel: +86-10-82544821

^bGraduate University of Chinese Academy of Sciences, Beijing 100049, China

^cSchool of Chemistry and Chemical Engineering, Guizhou University, Guiyang 550003, Guizhou, China

† Electronic supplementary information (ESI) available: The BET surface areas and pore diameters of the catalysts (Table S1), XPS data (Table S2), and the catalytic evaluation platform (Fig. S1). See DOI: 10.1039/c5ra07072d

and $Mn_xCo_{3-x}O_4$ nanocages as $DeNO_x$ catalysts.⁶⁷ Most recently, Kuang *et al.* have prepared novel porous Co_3O_4 nanocubes, which exhibit high specific surface area of $120.9\text{ m}^2\text{ g}^{-1}$, showing great efficiency in gas sensing applications.⁶⁸

To the best of our knowledge, porous Co_3O_4 supported Ru catalyst for complete oxidation of VOCs has not been reported. Therefore, it is necessary to investigate the preparation and application of porous Co_3O_4 supported Ru catalysts in oxidation of VOCs, such as toluene. Herein, porous Co_3O_4 was prepared using MOF-templated strategy, and its supported Ru material was obtained through impregnation method. Bulk Co_3O_4 and its corresponding Ru catalyst were also prepared for comparison. Tests were conducted to explore their catalytic activities in complete oxidation of toluene. The catalysts were characterized by BET, XRD, TEM, and XPS to study their physicochemical properties, which correspond with their catalytic activities.

2. Experimental section

2.1. Catalyst preparation

Co-MOF (ZIF-67) and porous Co_3O_4 were synthesized following the procedure described in the literature with some modifications.⁶⁸ In a typical preparation, a 12 mL aqueous solution of $Co(NO_3)_2 \cdot 6H_2O$ (1.75 g, 6 mmol) was added to a 80 mL aqueous solution of 2-methylimidazole (21.30 g, 260 mmol), and the mixture was stirred for 6 h at room temperature. The resulting purple precipitates were collected by centrifugation, and washed with water for 3 times and alcohol for 3 times, respectively. The obtained Co-MOF (ZIF-67) was dried at $80\text{ }^\circ\text{C}$ overnight. The as-prepared Co-MOF (ZIF-67) precursor was loaded in a ceramic crucible and then calcined in a muffle furnace at a ramp of $5\text{ }^\circ\text{C min}^{-1}$ from $30\text{ }^\circ\text{C}$ to $325\text{ }^\circ\text{C}$ and kept at this temperature for 3 h, giving a black powder, which was denoted as Co_3O_4 -MOF.

Supported 1 wt% Ru/ Co_3O_4 -MOF catalyst was prepared by impregnation method. The as-prepared Co_3O_4 -MOF support was impregnated with an aqueous solution containing an appropriate amount of $Ru(NO)(NO_3)_3$, and then dried at $80\text{ }^\circ\text{C}$ for 6 h and calcined at $325\text{ }^\circ\text{C}$ for 3 h.

Bulk Co_3O_4 -B sample was prepared using precipitation method with $Co(NO_3)_2 \cdot 6H_2O$ and Na_2CO_3 as reagents.⁵⁸ The resulting precipitates were dried at $80\text{ }^\circ\text{C}$ for 6 h and calcined at $325\text{ }^\circ\text{C}$ for 3 h, affording bulk Co_3O_4 -B. Impregnation of Co_3O_4 -B with an aqueous solution containing an appropriate amount of $Ru(NO)(NO_3)_3$ followed by calcination at $325\text{ }^\circ\text{C}$ for 3 h gave 1 wt% Ru/ Co_3O_4 -B.

2.2. Catalyst characterization

Physicochemical properties of the catalysts were characterized by means of techniques. X-ray diffraction (XRD) patterns of the samples were recorded on a powder diffractometer (Rigaku D/Max-RA) using $Cu\text{ K}\alpha$ radiation (40 kV and 120 mA). The porous texture was characterized by N_2 adsorption at 77 K in an automatic surface area and porosity analyzer (Autosorb iQ, Quantachrome). Transmission electron microscopy (TEM) and high resolution transmission electron microscopy (HR-TEM)

were taken on a Tecnai G2 F20 S-TWIN field emission transmission electron microscope operated at 200 kV. X-ray photoelectron spectroscopy (XPS) measurements were conducted on a Thermo escalab 250Xi X-ray using $Al\text{ K}\alpha$ source.

2.3. Catalytic evaluation

Catalytic activities of the catalysts were evaluated in a continuous flow fixed-bed quartz microreactor (i.d. = 4 mm) from 100 to $300\text{ }^\circ\text{C}$ with 100 mg of catalyst (80–100 mesh). Toluene was introduced into reactant flow by Ar through a saturator, and its concentration in the total flow of the reactant mixture (1000 ppm toluene + 20% O_2 + Ar (balance)) was calibrated by GC through a by-pass (Fig. S1†). The total flow ratio of the reactant mixture was 100 mL min^{-1} with the weight hourly space velocity (WHSV) of $60\text{ }000\text{ mL g}^{-1}\text{ h}^{-1}$. Before the test, the sample was pretreated at $250\text{ }^\circ\text{C}$ in a 20% O_2 /Ar stream for 0.5 h. After the pretreatment, the reactant gas containing toluene was introduced to the reactor. Analysis of the reactants and products were performed on-line with a gas chromatography (GC 2010 Plus, Shimadzu) equipped with a flame ionization detector (FID) and the concentration of CO_2 in the outlet gas was detected by another FID with a methanizer (MTN) furnace for converting CO_2 to CH_4 .

3. Results and discussion

3.1. Catalyst characterization

From the XRD patterns of the as-prepared Co_3O_4 samples in Fig. 1, it can be seen that these materials exhibited 31.4° , 36.9° , 38.2° , 44.8° , 59.4° , and 65.3° (2θ) peaks, which are attributable to standard Co_3O_4 sample (JCPDS PDF 43-1003). Any impurity phases such as Co, CoO, Co_2O_3 , and $Co(OH)_2$ were not observed. It should be noted that all diffraction peaks of the MOFs-templated samples are apparently broaden in width and weaken in intensity, indicating that the as-prepared materials are composed of abundant nanosized crystallites. The XRD patterns of Ru/ Co_3O_4 -MOF showed no obvious difference from those of Co_3O_4 -MOF, illustrating that Ru addition did not significantly change the formation of the nanostructure of Co_3O_4 -MOF.

The N_2 adsorption-desorption isotherms and BJH pore size distribution were performed to evaluate the specific surface area and the porosity of all the catalysts. As shown in Fig. 2, Co_3O_4 -MOF and Ru/ Co_3O_4 -MOF presented typical type IV adsorption isotherm with a H3-type hysteresis loop at a relative pressure range of 0.8–1.0, confirming the presence of a mesoporous structure. The specific surface area and pore size distribution of Ru/ Co_3O_4 -MOF were similar to those of Co_3O_4 -MOF (Fig. 2 and Table S1†). Obviously, MOFs-templated samples showed higher specific surface areas than the precipitation-resulted samples (Table S1†).

Fig. 3 showed the TEM images of Co_3O_4 -MOF and Ru/ Co_3O_4 -MOF samples. Slightly distorted nanocube was observed, retaining the initial morphology of the Co-MOFs precursors in some extent and confirming the successful preparation of expected materials. With the incorporation of Ru species, no

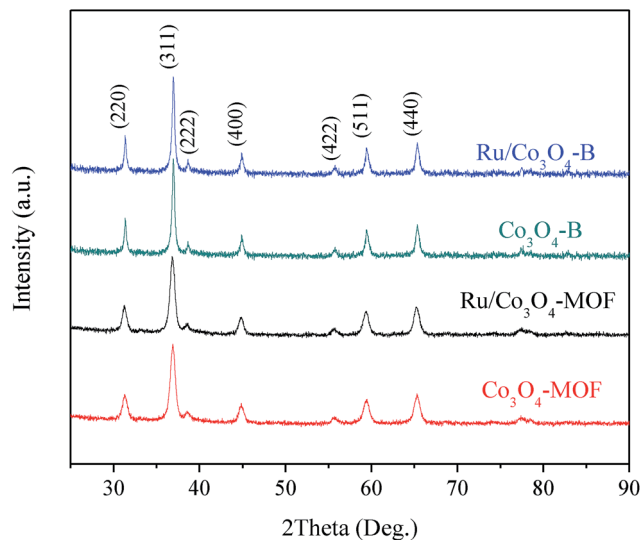


Fig. 1 XRD patterns of the catalysts.

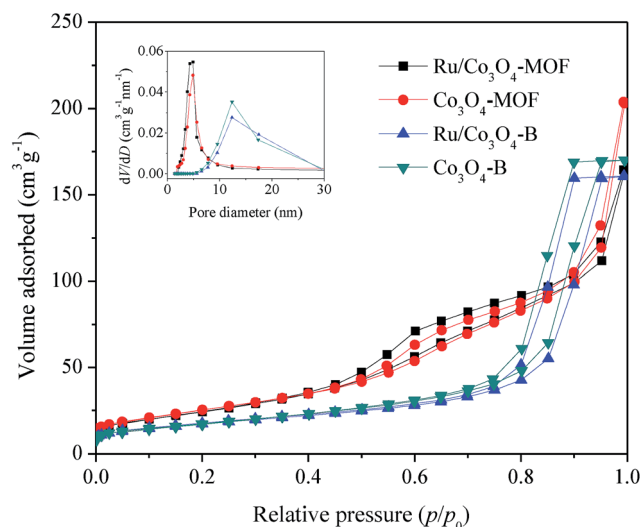


Fig. 2 N_2 adsorption-desorption isotherms and BJH pore size distributions of the catalysts.

apparent change of the nanostructure was observed for Ru/Co_3O_4-MOF . As shown in the high-resolution TEM images, 0.28 nm lattice spacing of Co_3O_4 (2 2 0) as well as 0.46 nm (1 1 1) lattice spacing were observed. For Co_3O_4 , the (1 1 1) planes were considered to be inactive crystal planes since they contain only Co^{2+} , which makes no contributions in the catalytic oxidation.³⁷ Ru/RuO_x nanoparticles were not observed in our HRTEM characterizations.

In order to analyze the chemical states of the Ru species, XPS characterizations for the Ru-containing samples were conducted, and the XPS spectra of Ru 3d were presented in Fig. 4. It can be seen that the samples exhibited three Ru $3d_{5/2}$ peaks at 280.8, 281.9, and 282.8 eV, which could be assigned to Ru^0 , Ru^{4+} , and Ru^{6+} , respectively.⁵³ Apparently, the oxidic Ru species dominate in both catalysts. The ratio of Ru^{4+}/Ru^{6+} for Ru/Co_3O_4-

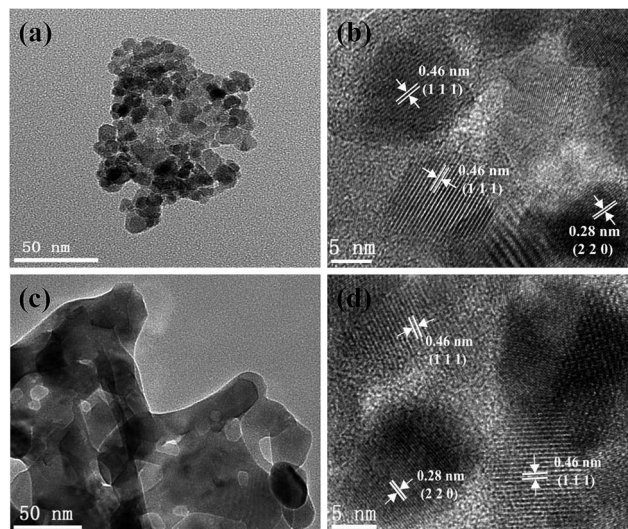


Fig. 3 TEM and HRTEM images of the catalysts: (a and b) Co_3O_4-MOF , (c and d) Ru/Co_3O_4-MOF .

MOF is 2.0, higher than that of Ru/Co_3O_4-B (1.36). Ru/Co surface atomic ratios of Ru/Co_3O_4-MOF and Ru/Co_3O_4-B were 0.038 and 0.013, revealing that Ru/Co_3O_4-MOF exhibits a higher Ru dispersion (Table S2†).

3.2. Catalytic studies

The catalytic efficiencies of the catalysts for the oxidation of toluene at a WHSV of $60\ 000\ mL\ g^{-1}\ h^{-1}$ are shown in Fig. 5. It can be easily seen that Co_3O_4-MOF showed better catalytic activity than Co_3O_4-B , illustrating that the porous nanostructure facilitates the complete oxidation of toluene. Among the as-prepared catalysts, Ru/Co_3O_4-MOF gave the lowest T_{90} of $238\ ^\circ C$, which is much lower than those of other catalysts, and its catalytic activity was comparable to reported 1 wt% Pd-loaded catalysts with the T_{90} temperature range of $212-258\ ^\circ C$ in the oxidation of toluene.^{69,70} Noteworthy, Co_3O_4-MOF

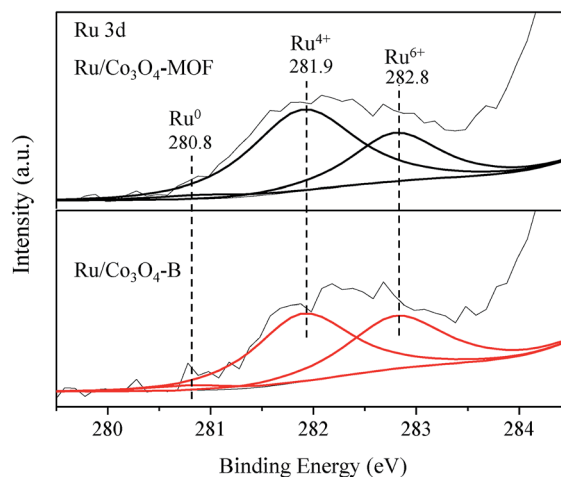


Fig. 4 XPS spectra of Ru 3d for Ru/Co_3O_4-MOF and Ru/Co_3O_4-B .

showed a lower T_{90} (264 °C) than that of Ru/Co₃O₄-B (286 °C), demonstrating that the porous support itself exhibits great catalytic activity possibly due to its unique nanostructural properties which are favorable for the adsorption and diffusion of the toluene molecules.

CO₂ selectivity represents an important performance of a catalyst for catalytic oxidation of VOCs. Accordingly, herein CO₂ selectivity was examined for both Ru/Co₃O₄-MOF and Co₃O₄-MOF materials, and the results were illustrated in Fig. 6. Using Ru/Co₃O₄-MOF as the catalyst, CO₂ and H₂O were the only products, and CO₂ selectivity was above 99.9%, revealing that toluene could be completely oxidized over this sample. For comparison, Co₃O₄-MOF catalyst was also employed under the same conditions. Along with the increase of temperature from 200 °C to 275 °C, small amount CO was observed. The CO₂ selectivity rised from 91% to 100%, and no other organic species were observed.

Water vapor exists in the VOCs-contained flue gases with a percentage level. Hence, we conducted the catalytic oxidation of toluene in presence of 1.5 vol% water vapor to examine the effect of water vapor on the catalytic performance. The most effective material of Ru/Co₃O₄-MOF was utilized as the catalyst. As shown in Fig. 7, when the temperature was raised to 235 °C, the conversion decreased from 86% to 79% within the 1st hour, possibly due to the actual higher temperature on the surface of the catalyst resulted from the unbalanced heat release. Then, the conversion smoothly increased from 79% to 84% in the next 2 h. Addition of water vapor led to a sharp decrease of toluene conversion by *ca.* 30%. Interestingly, when water vapor was cut off, the catalyst showed apparent higher catalytic efficiency than before. It was tentatively proposed that water facilitates the dispersion of Ru/RuO₂, whereas water occupies the active sites of the catalyst leading to the inhibition effect. When abundant water was introduced to the system, the inhibition effect played a major role. When the water vapor was cut off, higher

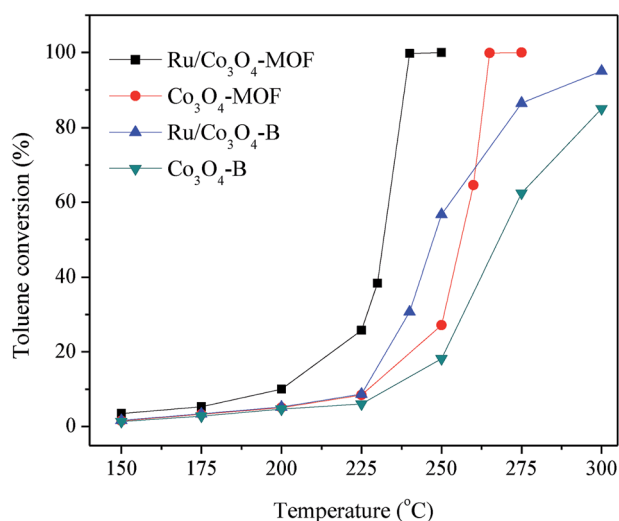


Fig. 5 Toluene conversion as a function of reaction temperature over the catalysts under the conditions of toluene concentration = 1000 ppm, toluene/O₂ molar ratio = 1/200, and WHSV = 60 000 mL g⁻¹ h⁻¹.

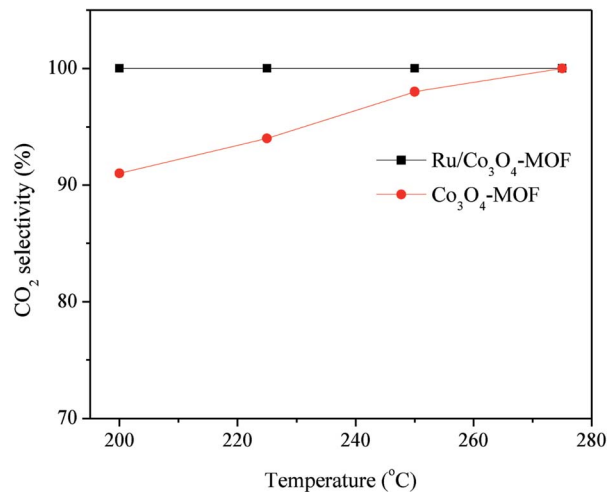


Fig. 6 CO₂ selectivity at different temperatures over Ru/Co₃O₄-MOF and Co₃O₄-MOF catalysts under the conditions of toluene concentration = 1000 ppm, toluene/O₂ molar ratio = 1/200, and WHSV = 60 000 mL g⁻¹ h⁻¹.

dispersion of Ru species led to an apparent promotion effect. For the reaction conducted at 245 °C, the introduction of water vapor barely influence the catalytic activity of Ru/Co₃O₄-MOF.

To evaluate the catalytic stability, on-stream toluene oxidation experiment was performed at 230 °C and 240 °C, respectively. The results are shown in Fig. 8. When the temperature was 230 °C, the toluene conversion decreased slowly within the 1st hour. Then, the conversion showed a slightly increasing tendency, revealing that the catalytic activity became higher with time extension. When the reaction temperature was raised to 240 °C, the toluene conversion sharply increased to 95.6%. Over time, an equivalent conversion was obtained, and no

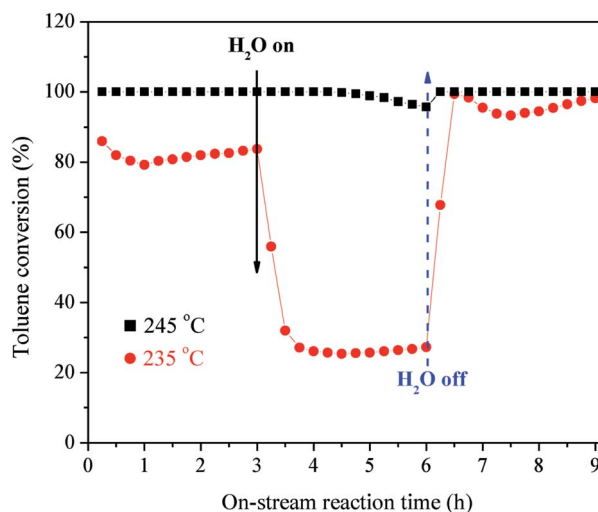


Fig. 7 Effect of water vapor on toluene conversion at different temperatures over Ru/Co₃O₄-MOF catalyst under the conditions of toluene concentration = 1000 ppm, toluene/O₂ molar ratio = 1/200, water vapor concentration = 1.5 vol%, and WHSV = 60 000 mL g⁻¹ h⁻¹.

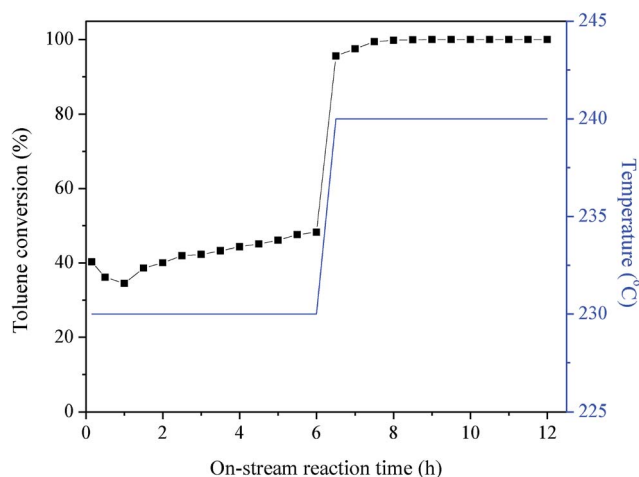


Fig. 8 Toluene conversion as a function of on-stream reaction time at 230 °C and 240 °C over the Ru/Co₃O₄-MOF catalyst under the conditions of toluene concentration = 1000 ppm, toluene/O₂ molar ratio = 1/200, and WHSV = 60 000 mL g⁻¹ h⁻¹.

significant loss in catalytic activity was detected, demonstrating that the Ru/Co₃O₄-MOF sample was catalytically durable.

4. Conclusions

Porous Co₃O₄ was prepared through MOFs-templated method, and its supported ruthenium catalyst was synthesized by impregnation. These materials showed larger BET surface areas than the bulk materials resulted from precipitation method. The BJH pore diameters of Ru/Co₃O₄-MOF and Co₃O₄-MOF were 4.9 nm, revealing a mesoporous structure. Catalytic oxidation of toluene over these materials was conducted. For Ru/Co₃O₄-MOF sample, complete oxidation of toluene was observed at 240 °C, showing a highest catalytic activity. Within the temperature range of 200–275 °C, the CO₂ selectivity was above 99.9% for Ru/Co₃O₄-MOF. In the stability tests, slowly increasing toluene conversion was observed. Additionally, water vapor showed an inhibition effect for the toluene oxidation at 235 °C. However, the catalytic activity became better when water vapor was cut off. The inhibition effect almost disappeared at a relatively higher temperature of 240 °C, and the toluene conversion basically maintained at 100%, demonstrating a great water-resistance for Ru/Co₃O₄-MOF.

Acknowledgements

This work was supported by the State 863 project (no. 2012AA062803).

Notes and references

- J. I. Gutiérrez-Ortiz, B. de Rivas, R. López-Fonseca and J. R. González-Velasco, *Appl. Catal., B*, 2006, **65**, 191–200.
- D. T. Tefera, Z. Hashisho, J. H. Philips, J. E. Anderson and M. Nichols, *Environ. Sci. Technol.*, 2014, **48**, 5108–5117.

- S. Xia, H. Zhu, H. Cai, J. Zhang, J. Yu and Z. Tang, *RSC Adv.*, 2014, **4**, 57975–57982.
- K. Everaert and J. Baeyens, *J. Hazard. Mater.*, 2004, **109**, 113–139.
- C. Kennes, E. R. Rene and M. C. Veiga, *J. Chem. Technol. Biotechnol.*, 2009, **84**, 1419–1436.
- S. Mudliar, B. Giri, K. Padoley, D. Satpute, R. Dixit, P. Bhatt, R. Pandey, A. Juwarkar and A. Vaidya, *J. Environ. Manage.*, 2010, **91**, 1039–1054.
- A. M. Vandembroucke, R. Morent, N. De Geyter and C. Leys, *J. Hazard. Mater.*, 2011, **195**, 30–54.
- A. Celebioglu and T. Uyar, *RSC Adv.*, 2013, **3**, 22891–22895.
- L. Kuboňová, L. Obalová, L. Skovranek and I. Troppová, *Adsorption*, 2013, **19**, 667–673.
- S. Ojala, S. Pitkääho, T. Laitinen, N. N. Koivikko, R. Brahmī, J. Gáalová, L. Matejova, A. Kucherov, S. Päivärinta, C. Hirschmann, T. Nevanperä, M. Riihimäki, M. Pirilä and R. L. Keiski, *Top. Catal.*, 2011, **54**, 1224–1256.
- S. Scire and L. F. Liotta, *Appl. Catal., B*, 2012, **125**, 222–246.
- L. F. Liotta, *Appl. Catal., B*, 2010, **100**, 403–412.
- M. Hosseini, T. Barakat, R. Cousin, A. Aboukais, B. L. Su, G. De Weireld and S. Siffert, *Appl. Catal., B*, 2012, **111**, 218–224.
- S. Pitkääho, T. Nevanperä, L. Matejova, S. Ojala and R. L. Keiski, *Appl. Catal., B*, 2013, **138**, 33–42.
- T. Barakat, V. Idakiev, R. Cousin, G. S. Shao, Z. Y. Yuan, T. Tabakova and S. Siffert, *Appl. Catal., B*, 2014, **146**, 138–146.
- W. B. Li, J. X. Wang and H. Gong, *Catal. Today*, 2009, **148**, 81–87.
- L. F. Liotta, M. Ousmane, G. Di Carlo, G. Pantaleo, G. Deganello, A. Boreave and A. Giroir-Fendler, *Catal. Lett.*, 2009, **127**, 270–276.
- Z. Özcelik, G. S. P. Soylu and I. Boz, *Chem. Eng. J.*, 2009, **155**, 94–100.
- C. He, Y. K. Yu, C. W. Chen, L. Yue, N. L. Qiao, Q. Shen, J. S. Chen and Z. P. Hao, *RSC Adv.*, 2013, **3**, 19639–19656.
- M. H. Castaño, R. Molina and S. Moreno, *Appl. Catal., A*, 2015, **492**, 48–59.
- R. Spinicci, M. Faticanti, P. Marini, S. De Rossi and P. Porta, *J. Mol. Catal. A: Chem.*, 2003, **197**, 147–155.
- B. P. Barbero, J. A. Gamboa and L. E. Cadús, *Appl. Catal., B*, 2006, **65**, 21–30.
- M. C. Álvarez-Galván, V. A. de la Peña O'Shea, G. Arzamendi, B. Pawelec, L. M. Gandía and J. L. G. Fierro, *Appl. Catal., B*, 2009, **92**, 445–453.
- H. Einaga, S. Hyodo and Y. Teraoka, *Top. Catal.*, 2010, **53**, 629–634.
- C. Zhang, Y. Guo, Y. Guo, G. Lu, A. Boreave, L. Retailleau, A. Baylet and A. Giroir-Fendler, *Appl. Catal., B*, 2014, **148**, 490–498.
- T. Mitsui, K. Tsutsui, T. Matsui, R. Kikuchi and K. Eguchi, *Appl. Catal., B*, 2008, **78**, 158–165.
- H. L. Tidahy, M. Hosseni, S. Siffert, R. Cousin, J. F. Lamonier, A. Aboukais, B. L. Su, J. M. Giraudon and G. Leclercq, *Catal. Today*, 2008, **137**, 335–339.

- 28 N. Kamiuchi, T. Mitsui, N. Yamaguchi, H. Muroyama, T. Matsui, R. Kikuchi and K. Eguchi, *Catal. Today*, 2010, **157**, 415–419.
- 29 T. Barakat, J. C. Rooke, M. Franco, R. Cousin, J. F. Lamonier, J. M. Giraudon, B. L. Su and S. Siffert, *Eur. J. Inorg. Chem.*, 2012, 2812–2818.
- 30 Z. S. Liu, J. Y. Chen and Y. H. Peng, *J. Hazard. Mater.*, 2013, **256**, 49–55.
- 31 C. Cellier, V. Ruaux, C. Lahousse, P. Grange and E. M. Gaigneaux, *Catal. Today*, 2006, **117**, 350–355.
- 32 F. G. Durán, B. P. Barbero, L. E. Cadús, C. Rojas, M. A. Centeno and J. A. Odriozola, *Appl. Catal., B*, 2009, **92**, 194–201.
- 33 Z. Wang, G. Shen, J. Li, H. Liu, Q. Wang and Y. Chen, *Appl. Catal., B*, 2013, **138**, 253–259.
- 34 J. Łojewska, A. Kołodziej, J. Zak and J. Stoch, *Catal. Today*, 2005, **105**, 655–661.
- 35 S. Albonetti, R. Bonelli, R. Delaigle, C. Femoni, E. M. Gaigneaux, V. Morandi, L. Ortolani, C. Tiozzo, S. Zacchini and F. Trifirò, *Appl. Catal., A*, 2010, **372**, 138–146.
- 36 Y. Wang, C. Zhang, F. Liu and H. He, *Appl. Catal., B*, 2013, **142**, 72–79.
- 37 Y. Liu, H. Dai, J. Deng, S. Xie, H. Yang, W. Tan, W. Han, Y. Jiang and G. Guo, *J. Catal.*, 2014, **309**, 408–418.
- 38 F. Gao and D. W. Goodman, *Phys. Chem. Chem. Phys.*, 2012, **14**, 6688–6697.
- 39 K. Qadir, S. H. Joo, B. S. Mun, D. R. Butcher, J. R. Renzas, F. Aksoy, Z. Liu, G. A. Somorjai and J. Y. Park, *Nano Lett.*, 2012, **12**, 5761–5768.
- 40 C. Mondelli, A. P. Amrute, F. Krumeich, T. Schmidt and J. Perez-Ramirez, *ChemCatChem*, 2011, **3**, 657–660.
- 41 G. Xiang, X. Shi, Y. Wu, J. Zhuang and X. Wang, *Sci. Rep.*, 2012, **2**, 801.
- 42 T. Mitsui, K. Tsutsui, T. Matsui, R. Kikuchi and K. Eguchi, *Appl. Catal., B*, 2008, **81**, 56–63.
- 43 S. Aouad, E. Abi-Aad and A. Aboukaïs, *Appl. Catal., B*, 2009, **88**, 249–256.
- 44 J. Okal and M. Zawadzki, *Appl. Catal., B*, 2009, **89**, 22–32.
- 45 N. Kamiuchi, T. Mitsui, H. Muroyama, T. Matsui, R. Kikuchi and K. Eguchi, *Appl. Catal., B*, 2010, **97**, 120–126.
- 46 J. Okal and M. Zawadzki, *Catal. Lett.*, 2009, **132**, 225–234.
- 47 J. Okal and M. Zawadzki, *Appl. Catal., B*, 2011, **105**, 182–190.
- 48 J. Okal, M. Zawadzki and W. Tylus, *Appl. Catal., B*, 2011, **101**, 548–559.
- 49 S. Aouad, E. Saab, E. Abi-Aad and A. Aboukaïs, *Kinet. Catal.*, 2007, **48**, 835–840.
- 50 Q. Dai, S. Bai, Z. Wang, X. Wang and G. Lu, *Appl. Catal., B*, 2012, **126**, 64–75.
- 51 Q. Dai, S. Bai, J. Wang, M. Li, X. Wang and G. Lu, *Appl. Catal., B*, 2013, **142**, 222–233.
- 52 Q. Dai, S. Bai, X. Wang and G. Lu, *Appl. Catal., B*, 2013, **129**, 580–588.
- 53 H. Huang, Q. Dai and X. Wang, *Appl. Catal., B*, 2014, **158**, 96–105.
- 54 T. Mitsui, T. Matsui, R. Kikuchi and K. Eguchi, *Top. Catal.*, 2009, **52**, 464–469.
- 55 T. Garcia, S. Agouram, J. F. Sanchez-Royo, R. Murillo, A. M. Mastral, A. Aranda, I. Vázquez, A. Dejoz and B. Solsona, *Appl. Catal., A*, 2010, **386**, 16–27.
- 56 Y. Xia, H. Dai, H. Jiang and L. Zhang, *Catal. Commun.*, 2010, **11**, 1171–1175.
- 57 B. de Rivas, R. López-Fonseca, C. Jiménez-González and J. I. Gutiérrez-Ortiz, *J. Catal.*, 2011, **281**, 88–97.
- 58 L. F. Liotta, H. Wu, G. Pantaleo and A. M. Venezia, *Catal. Sci. Technol.*, 2013, **3**, 3085–3102.
- 59 L. F. Liotta, M. Ousmane, G. Di Carlo, G. Pantaleo, G. Deganello, G. Marci, L. Retailleau and A. Giroir-Fendler, *Appl. Catal., A*, 2008, **347**, 81–88.
- 60 Q. Liu, L. C. Wang, M. Chen, Y. Cao, H. Y. He and K. N. Fan, *J. Catal.*, 2009, **263**, 104–113.
- 61 J. Łojewska, A. Kołodziej, T. Łojewski, R. Kapica and J. Tyczkowski, *Appl. Catal., A*, 2009, **366**, 206–211.
- 62 F. Wyrwalski, J. M. Giraudon and J. F. Lamonier, *Catal. Lett.*, 2010, **137**, 141–149.
- 63 Q. Yan, X. Li, Q. Zhao and G. Chen, *J. Hazard. Mater.*, 2012, **209**, 385–391.
- 64 X. Xu, R. Cao, S. Jeong and J. Cho, *Nano Lett.*, 2012, **12**, 4988–4991.
- 65 T. K. Kim, K. J. Lee, J. Y. Cheon, J. H. Lee, S. H. Joo and H. R. Moon, *J. Am. Chem. Soc.*, 2013, **135**, 8940–8946.
- 66 F. Meng, Z. Fang, Z. Li, W. Xu, M. Wang, Y. Liu, J. Zhang, W. Wang, D. Zhao and X. Guo, *J. Mater. Chem. A*, 2013, **1**, 7235–7241.
- 67 L. Zhang, L. Y. Shi, L. Huang, J. P. Zhang, R. H. Gao and D. S. Zhang, *ACS Catal.*, 2014, **4**, 1753–1763.
- 68 Y. Lü, W. Zhan, Y. He, Y. Wang, X. Kong, Q. Kuang, Z. Xie and L. Zheng, *ACS Appl. Mater. Interfaces*, 2014, **6**, 4186–4195.
- 69 P. Li, C. He, J. Cheng, C. Ma, B. Dou and Z. Hao, *Appl. Catal., B*, 2011, **101**, 570–579.
- 70 C. He, Q. shen and M. Liu, *J. Porous Mater.*, 2014, **21**, 551–563.